

Repurposing Tamoxifen for Tumor Microenvironment Priming and Enhanced Tumor-Targeted Drug Delivery

Ilaria Biancacci, Daniele De Santis, Elena Rama, Karina Benderski, Jeffrey Momoh, Robert Pohlberger, Diana Moeckel, Leonard Kaps, Cristianne J. F. Rijcken, Jai Prakash, Marielle Thewissen, Fabian Kiessling, Yang Shi, Quim Peña, Alexandros Marios Sofias, Lorena Consolino,* and Twan Lammers*


The dense stromal matrix in fibrotic tumors hinders tumor-targeted drug delivery. Tamoxifen (TMX), an estrogen receptor modulator that is clinically used for the treatment of breast cancer, is shown to reprogram the tumor microenvironment (TME) and to alleviate desmoplasia. It is investigated if TMX, administered in free and nano-formulated form, can be repurposed as a TME remodeling agent to improve tumor accumulation of nano-formulations in pancreatic ductal adenocarcinoma and triple-negative breast cancer mouse models, evaluated using clinical-stage Cy7-labeled core-crosslinked polymeric micelles (CCPM). Under control conditions, higher levels of Cy7-CCPM are found in PANC-1 tumors (16.7% ID g^{-1} at 48 h post i.v. injection) than in 4T1 tumors (11.0% ID g^{-1}). In both models, free and nano-formulated TMX failed to improve CCPM delivery. These findings are congruent with the results from histopathological immunofluorescence analysis of tumor tissue, which indicate that TMX treatment does not significantly change vascularization, perfusion, macrophage infiltration, collagen density, and collagen fiber thickness. Altogether, these results demonstrate that in PANC-1 and 4T1 mouse models, TMX treatment does not contribute to beneficial TME priming and enhanced tumor-targeted drug delivery.

1. Introduction

The tumor microenvironment (TME) plays a key role in tumor growth, metastasis, drug delivery, and resistance to therapy.^[1] One of the major challenges in cancer therapy is to efficiently target drugs to tumor cells while sparing healthy tissues. Recent insights indicate that the TME interferes with drug penetration, thus limiting drug access to cancer cells and the efficacy of anti-cancer drug therapy.^[2] The TME is typically characterized by a dense extracellular matrix (ECM), mainly composed of collagen.^[3] The compactness of the matrix is exacerbated in fibrotic tumors and results from excessive deposition of collagen fibers, produced by hyper-activated cancer-associated fibroblasts (CAFs).^[4,5] This dense ECM limits the penetration of drugs and drug delivery systems out of the blood vessels into the tumor interstitium.^[6,7] Increased ECM deposition can furthermore result in compression of tumor blood vessels,^[8] thereby

I. Biancacci, D. De Santis, E. Rama, K. Benderski, J. Momoh, R. Pohlberger, D. Moeckel, Y. Shi, Q. Peña, A. M. Sofias, L. Consolino, T. Lammers
Department of Nanomedicine and Theranostics
Institute for Experimental Molecular Imaging
RWTH Aachen University
Forckenbeckstrasse 55, 52074 Aachen, Germany
E-mail: lconsolino@ukaachen.de; tlammers@ukaachen.de
D. De Santis
Department of Biomolecular Sciences
University of Urbino
Piazza Rinascimento 6, Urbino 61029, Italy

L. Kaps
Department of Internal Medicine 1
University Medical Center of the Johannes Gutenberg-University Mainz
Langenbeckstrasse 1, 55131 Mainz, Germany
L. Kaps
Institute of Translational Immunology and Research Center for Immunotherapy/FZI
University Medical Center of the Johannes Gutenberg-University Mainz
Obere Zahlbacher Str. 63, 55131 Mainz, Germany
C. J. F. Rijcken, M. Thewissen
Cristal Therapeutics
Oxfordlaan 55, Maastricht 6229 EV, The Netherlands
J. Prakash
Engineered Therapeutics Section, Department of Advanced Organ Bioengineering and Therapeutics, Technical Medical Centre
University of Twente
Drienerlolaan 5, Enschede 7522 NB, The Netherlands
F. Kiessling
Institute for Experimental Molecular Imaging
RWTH Aachen University
Forckenbeckstrasse 55, 52074 Aachen, Germany

 The ORCID identification number(s) for the author(s) of this article can be found under <https://doi.org/10.1002/adtp.202300098>

© 2023 The Authors. Advanced Therapeutics published by Wiley-VCH GmbH. This is an open access article under the terms of the Creative Commons Attribution-NonCommercial License, which permits use, distribution and reproduction in any medium, provided the original work is properly cited and is not used for commercial purposes.

DOI: 10.1002/adtp.202300098

reducing tumor perfusion and hindering efficient drug access to and distribution in tumors, particularly in desmoplastic tumors such as in pancreatic cancer and certain types of breast cancer.^[9–12] Altogether, the stromal nature of the TME results in poor drug therapy outcomes for patients.

Several pharmacological and physical strategies aiming at modulating the TME to alleviate tumor fibrosis have been shown to improve the delivery and efficacy of drugs and drug nanoformulations.^[13–15] Many TME remodeling strategies have specifically focused on nanomedicine formulations, such as liposomes and micelles.^[16–19] Nanomedicines can accumulate in tumors relatively effectively and selectively, thereby improving therapeutic performance and minimizing side effects.^[20,21] TME-priming nanomedicines have been loaded with enzymes that break down ECM structures (e.g., collagenase and hyaluronidase),^[22–24] as well as with compounds that interfere with ECM synthesis and deposition.^[25,26] Nanomedicine formulations have furthermore been co-loaded with TME-modulating agents and chemotherapeutic drugs, together typically resulting in enhanced tumor accumulation and potentiation of therapeutic responses.^[23,27,28]

In parallel to the development of novel TME-remodeling drugs and nanomedicines, various agents clinically approved for other diseases or medical conditions are currently being explored for repurposing as antifibrotic agents in cancer therapy.^[17,29–33] Tamoxifen (TMX) is a pharmacological modulator of the estrogen receptor (ER) clinically used for the treatment of ER-positive breast cancer.^[34] TMX is hypothesized to be such a TME remodeling agent. This is based on recent studies in which a novel mechanism of action of TMX—independent of the modulation of canonical ER signaling—has been identified, that is, the inhibition of CAF-mediated ECM deposition and tissue stiffening.^[35,36] In pancreatic cancer cell and mouse models, TMX inhibited collagen synthesis and collagen fibrils formation, reduced hypoxia and normalized the tumor vasculature.^[37] The sum of these findings suggests that TMX can potentially be repurposed as a TME-remodeling agent in pancreatic cancer and other stromal tumor types, in order to counteract tumor desmoplasia, and to thereby improve the tumor accumulation and antitumor efficacy of drugs and drug nanoformulations.

Based on the above notions, we set out to evaluate the efficacy of TMX as a TME modulator in two fibrotic mouse tumor models, that is, pancreatic adenocarcinoma (PDAC) and triple-negative breast cancer (TNBC). Taking into account the small size (<1 kDa) and high hydrophobicity (Log P = 6.35) of TMX, we employed a nano-formulation of TMX in addition to the free drug, in order to improve TMX pharmacokinetics, tumor accumulation and TME remodeling. To this end, we developed TMX-loaded π electron-stabilized polymeric micelles, based on methoxy-poly(ethylene glycol)-*b*-(*N*-(2-benzoyloxypropyl)methacrylamide), that is, mPEG-*b*-p(HPMAm-Bz).^[38,39] Upon free TMX and nano-TMX treatment for 2–3 weeks, we assessed the impact of potential TME priming via in vivo and ex vivo optical imaging of the tumor accumulation of Cy7-labeled core-crosslinked polymeric micelles

(CCPM) as clinically relevant nanocarriers. The CCPM employed in this study were based on CriPec and composed of chemically core-crosslinked methoxy-poly(ethylene glycol)-*b*-poly[*N*-(2-hydroxypropyl) methacrylamide lactate] (mPEG-*b*-pHPMAmLac_n) block copolymers.^[19,40] Changes in the composition of the TME in pancreatic and breast cancer mouse models induced by free and nanoformulated TMX treatment were finally analyzed via histopathological characterization of the tumors.

2. Results

2.1. Preparation and Characterization of TMX Micelles

TMX-loaded [mPEG-*b*-p(HPMAm-Bz)]-based micelles were generated by using the nano-precipitation method (schematic in **Figure 1A**).^[38] The developed micelles had a diameter of 58 nm and a polydispersity index (PDI) below 0.1, based on dynamic light scattering (DLS) measurements. The zeta potential was -0.1 mV. The encapsulation efficiency (EE) of TMX was 90%, as determined via high-performance liquid chromatography (HPLC), corresponding to a drug concentration of ≈ 1.8 mg mL⁻¹. The stability of the TMX-loaded micelles was evaluated for 7 days, at room temperature (RT) and at 4 °C. Neither the size nor the PDI changed over time (Figure 1B,C), and also the degree of drug loading (EE) remained constant (Figure 1D).

To simulate TMX release under physiological (sink) conditions, micelles were placed in a Float-A-Lyzer G2 dialysis bag, immersed in phosphate buffered saline (PBS) supplemented with 45 mg mL⁻¹ bovine serum albumin (BSA) at 37 °C. The TMX-loaded micelle dispersion was agitated for 4 days, until the amount of drug released reached a plateau. HPLC and DLS measurements were performed at different time points to determine drug retention and micelle size. More than 70% of TMX was retained within the micelles in the first 4 h upon agitation under sink conditions. After 4 days, 80% of the drug was found to be released (Figure 1E). The size of the micelles remained stable at around 60 nm during the whole experiment (Figure 1F).

To enable intravenous (i.v.) injection of nano-formulated TMX at comparable doses as administered intraperitoneally (i.p.), the micelles had to be concentrated prior to administration. This was done via centrifugation in a centrifugal concentrator at 4500 rpm for 20 min, eventually resulting in a 7-fold increase in concentration (12 mg mL⁻¹; Figure 1A), and enabling administration at a dose of 50 mg kg⁻¹ drug-equivalent dose via i.v. injection in the in vivo experiments.

2.2. CCPM Accumulation Upon TMX Priming in Pancreatic Tumors

The TME modulatory effects of TMX were first described in the PANC-1 pancreatic cancer tumor model. Accordingly, as depicted in the schematic in **Figure 2A**, we generated pancreatic tumor xenografts with a fibrotic phenotype by co-injecting PANC-1 cells together with CAF-precursors, that is, human primary pancreatic stellate cells (hPSC). From day 5 post tumor inoculation onwards, mice were treated with free and nano-formulated TMX every second day (Q2D) for 10 days, at a dose of 50 mg kg⁻¹

F. Kiessling
Fraunhofer Institute for Digital Medicine MEVIS
Max-Von-Laue-Strasse 2, 28359 Bremen, Germany

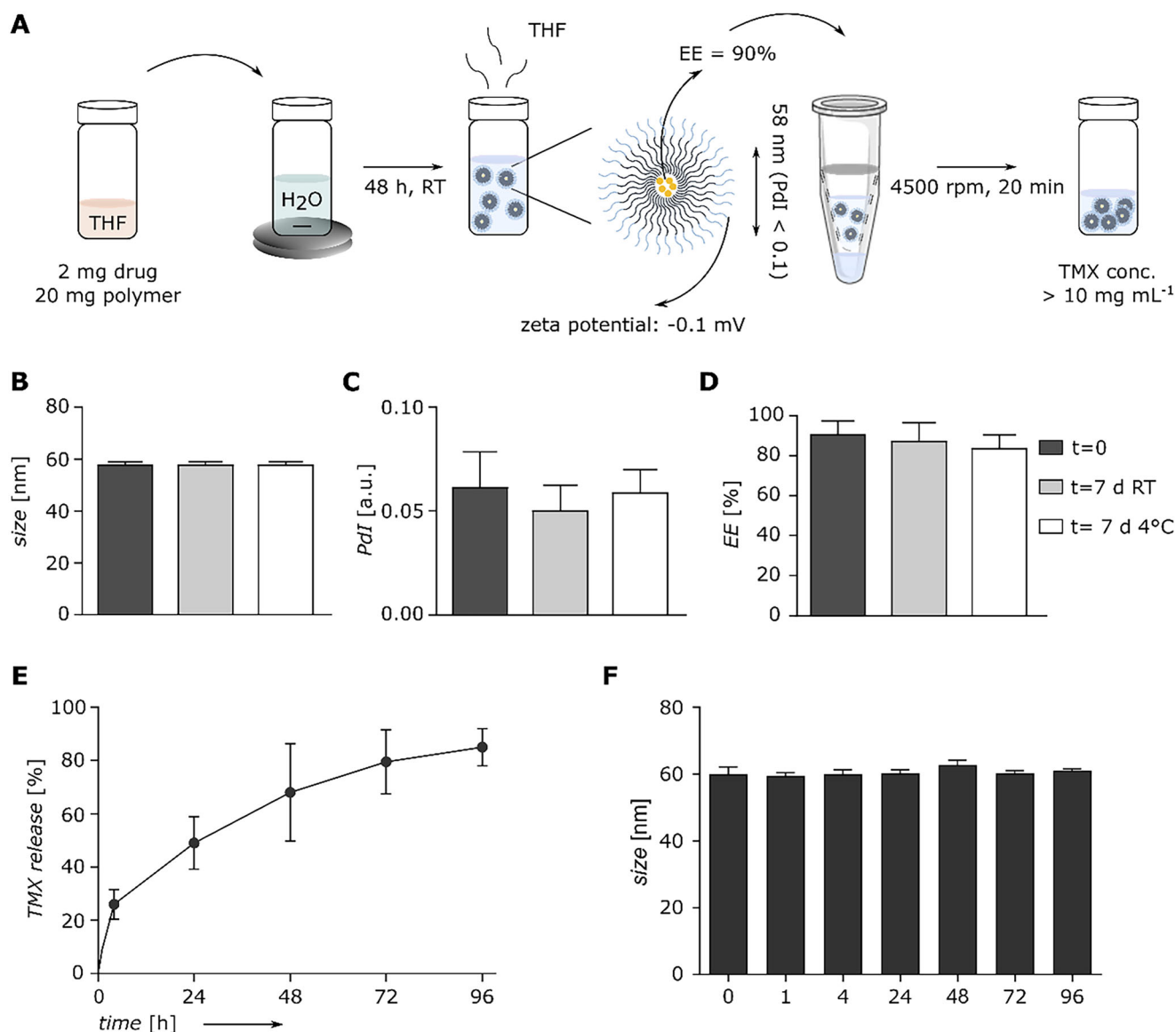


Figure 1. TMX micelles preparation and characterization. A) TMX micelles were prepared using the nano-precipitation method. To this end, TMX and mPEG-*b*-p(HPMAm-Bz) (1:10 w/w ratio) were dissolved in tetrahydrofuran (THF). The mixture was subsequently added to Milli-Q water under stirring and THF was left to evaporate for 48 h at RT. The resulting formulation (EE: 90%; size: 58 nm; PDI < 0.1; zeta potential: -0.1 mV) was concentrated using a centrifuge concentrator filter to reach a final TMX concentration of 12 mg mL^{-1} . B–D) TMX-micelles were kept at RT and at 4°C for 7 days, showing that they efficiently maintained their size, PDI, and drug content over time. E, F) Drug release and size of TMX-micelles were evaluated under sink conditions, in a continuously agitated PBS solution containing 45 mg mL^{-1} BSA at 37°C . Micelle size remained constant and the drug was found to be gradually released over 4 days.

drug-equivalent. The relative body weight of the mice was stable over the whole duration of the experiment (Figure 2B; absolute weights are provided in Figure S1A–C, Supporting Information), indicating decent tolerability. Somewhat unexpectedly, we found that tumors in mice treated with free or micelle-encapsulated TMX displayed slightly faster tumor growth as compared to controls (Figure 2C). In agreement with this, as shown in Figure S2A,B, Supporting Information, *in vivo* computed tomography (CT) imaging and non-invasive tumor volume determination also found slightly increased tumor sizes upon TMX treatment. However, the microscopic evaluation of Ki67 cell pro-

liferation marker in the tissues revealed no differences between the three groups (Figure S3A,B, Supporting Information).

To evaluate if TMX priming improves the delivery of nanomedicine formulations, Cy7-labeled CCPM were administered to the mice after five doses of free and micellar TMX, and their biodistribution and tumor accumulation were monitored *in vivo* at 0.25, 4, 24, and 48 h post *i.v.* injection. A representative 3D reconstruction of fused CT and fluorescence tomography (CT-FLI) data is shown in Figure 2D. The highest CCPM uptake levels were found for tumor, liver, and spleen (Figure S4, Supporting Information). When zooming in on

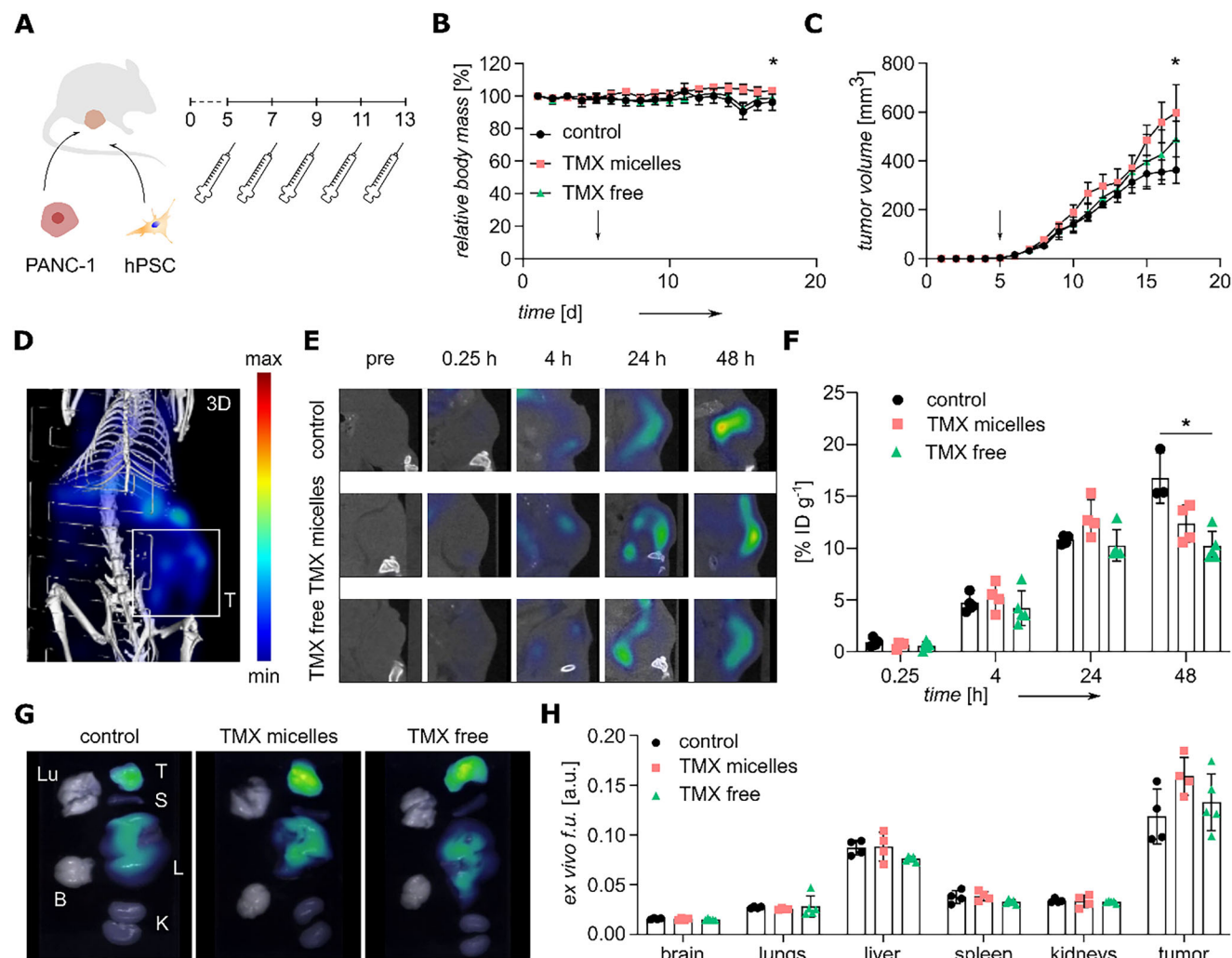


Figure 2. Effect of TMX priming on CCPM tumor accumulation in pancreatic cancer. A) PANC-1 pancreatic cancer cells and human primary pancreatic stellate cells (hPSC) were co-inoculated in a 1:1 ratio on day 0 in male BALB/c SCID mice. TMX was administered in micellar and free form at a dose of 50 mg kg^{-1} TMX-equivalent when tumors became palpable (day 5). Treatment was applied every two days for a total of five injections. B) Daily body weight monitoring showed good tolerability of the treatment. Arrow indicates start of therapy. * indicates $p < 0.05$ from day 15 onwards between TMX micelles and control group (based on unpaired nonparametric one-way ANOVA analysis with Dunn's multiple comparison test). C) Caliper-based tumor volumes determination, showing a slight but significant increase upon TMX treatment. * indicates $p < 0.05$ from day 11 onward between TMX micelles and control group (based on unpaired nonparametric one-way ANOVA analysis with Dunn's multiple comparison test). D,E) Representative CT-FLT images showing Cy7-CCPM biodistribution and tumor accumulation (indicated by T) at 0.25, 4, 24, and 48 h post i.v. injection. F) Quantification of Cy7-CCPM tumor concentration, normalized to the injected dose (ID) and expressed as a percentage of the injected dose per gram of tissue ($\% \text{ID g}^{-1}$) showing that free and micellar TMX do not enhance CCPM tumor targeting. * indicates $p = 0.012$ (based on unpaired nonparametric one-way ANOVA analysis with Dunn's multiple comparison test). G,H) Ex vivo FRI analysis of Cy7-CCPM accumulation in lung (Lu), tumor (T), spleen (S), liver (L), brain (B), and kidney (K), demonstrating a similar accumulation pattern for all three treatment groups, with CCPM predominantly present in tumor and liver, and with no obvious differences in tumor accumulation induced by TMX treatment.

tumor uptake (Figure 2E), no benefit of TMX priming treatment could be observed, with $16.7\% \text{ ID g}^{-1}$ found in tumors for the control group at 48 hours, as compared to $12.4\% \text{ ID g}^{-1}$ ($p = 0.439$) and $9.7\% \text{ ID g}^{-1}$ ($p = 0.012$) for the TMX micelles and TMX free groups, respectively (Figure 2F). The trends observed using semi-quantitative ex vivo fluorescence reflectance imaging (FRI) analysis of Cy7-CCPM fluorescence signals in tumors were in line with in vivo CT-FLT findings, showing potent CCPM tumor accumulation, but no added value of TMX priming treatment (Figure 2G,H).

2.3. TMX-Induced TME Remodeling in Pancreatic Tumors

We next investigated the impact of treatment with free and micellar TMX on the composition of the TME. Hereto, we first characterized tumors via analyzing hematoxylin and eosin (H&E) stained sections, noting that tumors in all groups exhibited a vast area of central necrosis (typically between 50% and 65% of the total area fraction; Figure S5, Supporting Information). Subsequently, we visualized and quantified TME components that are relevant for the drug delivery process, that is, collagen fibers,

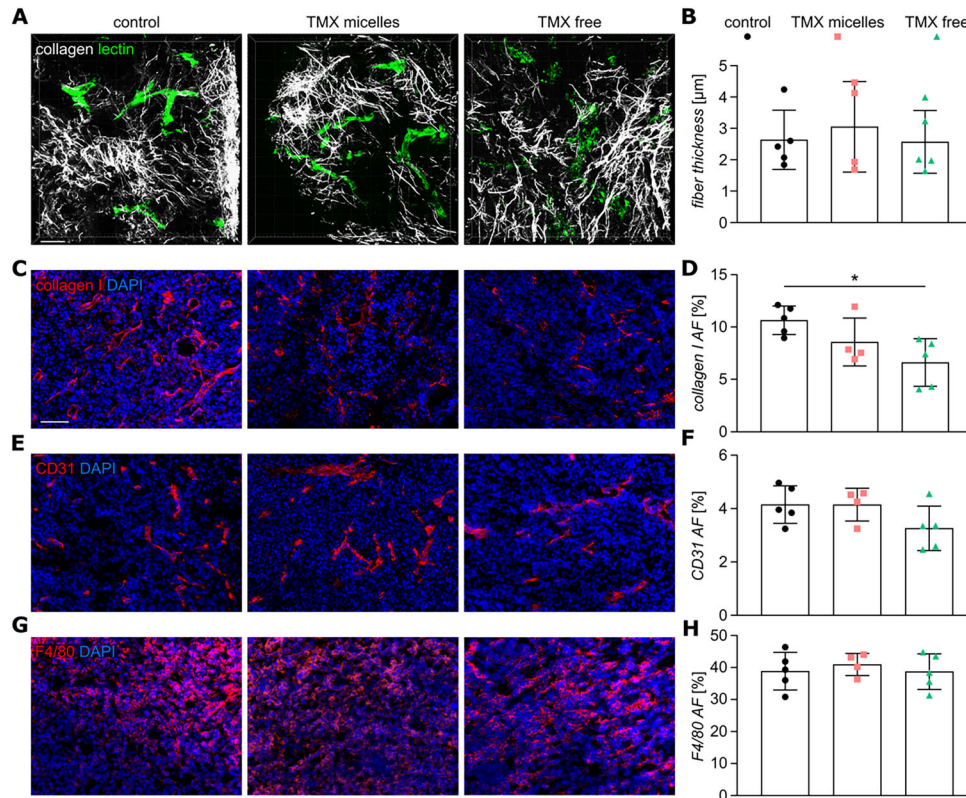


Figure 3. Effect of TMX treatment on the composition of the TME. A,B) Representative TPLSM images capturing collagen fibers via second harmonic generation (SHG) imaging and corresponding quantification showing similar collagen fiber thickness in all three groups. Scale bar corresponds to 60 μm. C,E,G) Representative fluorescence microscopy images of collagen I (C), CD31-positive endothelial cells (E), and F4/80-positive macrophages (G) in control and TMX-treated pancreatic tumors. Scale bar = 60 μm. D,F,H) Quantification of collagen I (D), CD31 (D), and F4/80 (F) area fraction (AF) shows very marginal changes in the composition of the TME upon TMX priming. * indicates $p = 0.021$ (based on unpaired nonparametric one-way ANOVA analysis with Dunn's multiple comparison test).

blood vessels and macrophages. Using immunofluorescence microscopy and two-photon laser scanning microscopy (TPLSM), we observed only very marginal differences for collagen fiber thickness between the three treatment groups, although significant differences were noticed between the collagen density in the control and TMX free groups (Figure 4A–D; Figure S6A,B, Supporting Information). The analysis of lysyl oxidase (LOX) enzyme, which plays a role in collagen crosslinking and matrix stiffness, showed comparable LOX content across all groups (Figure S3C,D, Supporting Information). Similar results among the groups were also observed for α SMA, a marker associated with activated cancer-associated fibroblasts (Figure S3E,F, Supporting Information). In addition, we analyzed the tumor vasculature by quantifying the area fraction of CD31 (vascular density) and lectin (vascular perfusion). Fluorescent microscopy showed a slight decrease of the CD31 signal upon treatment with free TMX (Figure 3E,F), although TPLSM displayed no differences in the perfusion volume between the tumors (Figure S6C, Supporting Information). Last, the amount of macrophages (F4/80-positive cells) remained unvaried between the three treatment groups, as evidenced by the fluorescence microscopy analysis (Figure 3G,H).

2.4. Effect of TMX Priming in a Triple-Negative Breast Cancer Mouse Model

The lack of effects of TMX treatment on the TME and tumor-directed delivery in the PANC-1 model was subsequently validated in a TNBC model. To this end, female BALB/cAnNRj mice were inoculated with 4T1 tumor cells and 3 days later they were randomized and assigned to the different treatment regimens (Figure 4A). The treatment with TMX was performed at the same dose, but treatment time was extended to 3 weeks (to increase the chances of observing TMX-associated TME priming effects; nine applications at 50 mg kg⁻¹ TMX-equivalents). Also at this dosing regimen, no toxicity was observed, as evidenced by the stable body weights of the mice during the course of the experiment (Figure 4B and Figure S1D–F, Supporting Information).

Similar to the previously shown PANC-1 pancreatic tumor model, the 4T1 TNBC tumors also displayed a slight but significant increase in size upon treatment with free and micellar TMX (Figure 4C and Figure S2C,D, Supporting Information), while comparable levels of Ki67 were observed in the treated versus untreated tumors (Figure S7A,B, Supporting Information). Representative CT-FLT images and the respective quantification of the

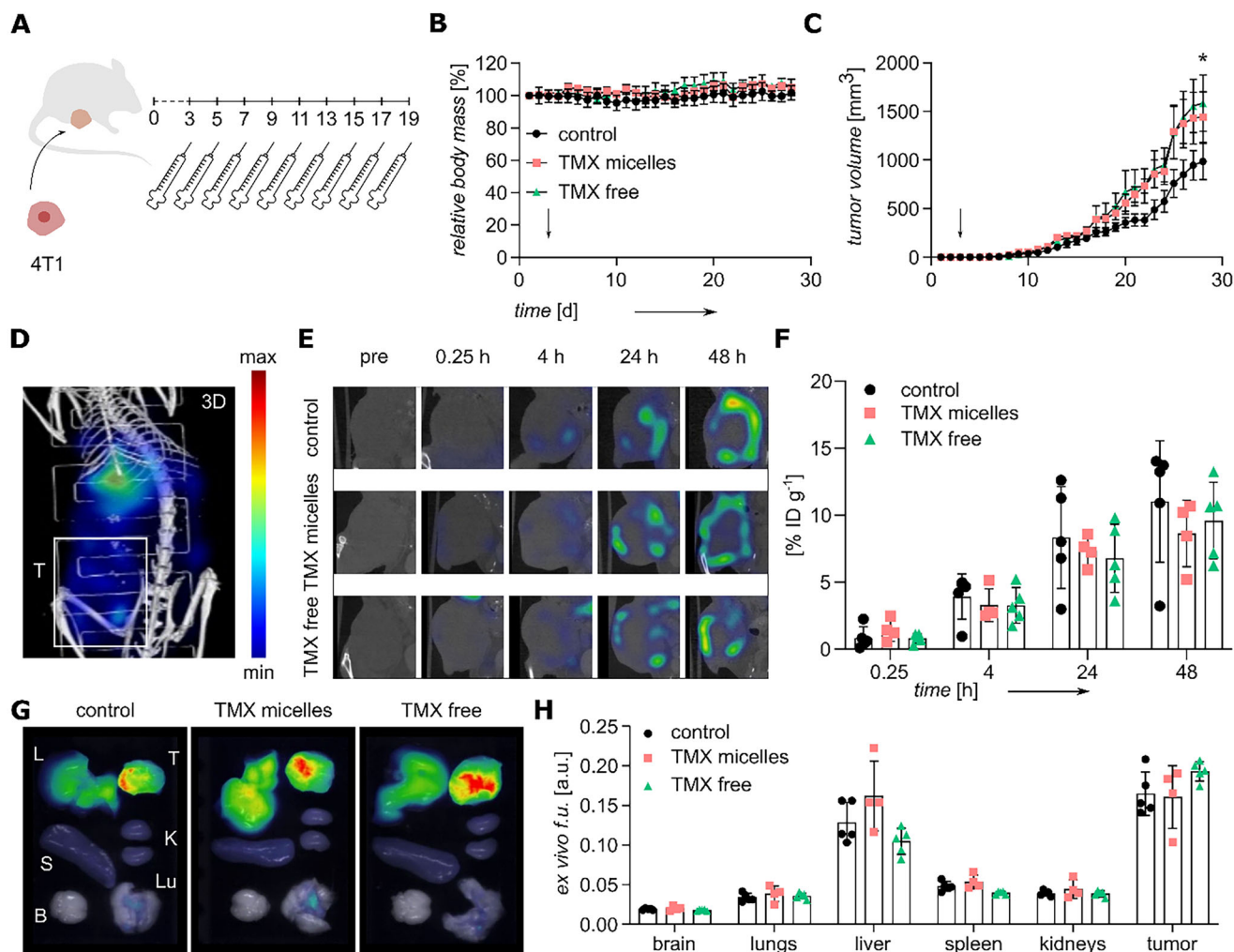


Figure 4. TMX treatment and CCPM accumulation in triple-negative breast cancer. A) 4T1 breast cancer cells were inoculated in female BALB/cAnNRj mice. TMX was administered in micellar and free form at a dose of 50 mg kg^{-1} when tumors were palpable (day 3). Treatment was applied every two days for a total of nine injections. B) Mouse body weights were recorded over 28 days. The arrow represents the start of the therapy. C) Caliper-based 4T1 tumor volume determination, showing a significant increase in tumor growth upon TMX treatment. * indicates $p < 0.05$ from day 11 onwards between TMX micelles and control groups, and from day 18 onwards between TMX free and control groups (based on unpaired nonparametric one-way ANOVA analysis with Dunn's multiple comparison test). D,E) Representative CT-FLT images showing Cy7-CCPM biodistribution and tumor accumulation (indicated by T) at 0.25, 4, 24, and 48 h post injection. F) Quantification of Cy7-CCPM tumor concentration, normalized to the injected dose (ID) and expressed as a percentage of the injected dose per gram of tissue ($\% \text{ID g}^{-1}$), showing that free and micellar TMX do not enhance CCPM tumor targeting. G,H) Ex vivo FRI analysis of Cy7-CCPM accumulation in lung (Lu), tumor (T), spleen (S), liver (L), brain (B), and kidney (K), exemplifying similar accumulation patterns for all three treatments groups.

fluorescent signals in the tumors are provided in Figure 4D–F. As compared to PANC-1 pancreatic tumors (Figure 2D–F), CCPM accumulation in TNBC was found to be somewhat lower, but in line with previous results in this model.^[40] In line with results obtained in PANC-1, no differences in CCPM accumulation were observed between the different treatment groups (Figure 4E,F). Ex vivo analysis of FRI images corroborated these findings, showing no enhancement of tumor accumulation by TMX, as well as the highest levels of CCPM accumulation in tumors, followed by liver and spleen (Figure 4G,H).

Histological characterization of 4T1 tumors showed a very mild remodeling of the TME upon treatment with TMX. The collagen I content analyzed via fluorescence microscopy, as well as

the average thickness of the collagen filaments analyzed via SHG in TPLSM, displayed a slight but statistically non-significant reduction upon TMX treatment (Figure 5A–D). Although no changes were observed in collagen content, the immunofluorescence staining for LOX indicates a reduction of collagen crosslinking in the TMX-treated groups, with a statistical significance for the TMX free group in comparison to the control group (Figure S7A,B, Supporting Information), while the maximum thickness of collagen fibers was not affected by the therapy (Figure S6E, Supporting Information). In addition, TMX-treated groups exhibited a slight reduction in αSMA levels, although these changes were not statistically significant (Figure S7E,F, Supporting Information). Tumors displayed a moderate increase

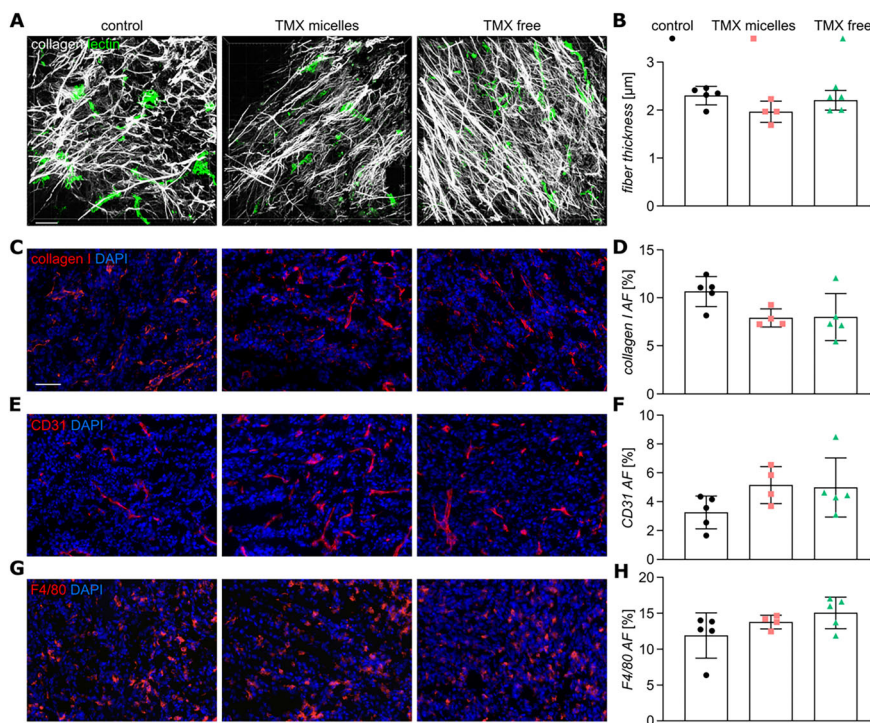


Figure 5. TMX-induced TME remodeling in triple-negative breast cancer. A,B) Analysis of collagen filaments acquired via SHG shows a slight but insignificant reduction in collagen density fibers upon TMX treatment. Scale bar is 60 μm. C,E,G) Representative fluorescence microscopy images showing collagen I (C), CD31-positive endothelial cells (E), and F4/80-positive macrophages (G) in control and TMX-treated 4T1 tumors. Scale bar equals 60 μm. D,F,H) Quantification of collagen I (D), CD31 (D), and F4/80 (F) area fraction shows very moderate changes in the composition of the TME upon TMX treatment. * indicates $p < 0.05$.

in vascularization and macrophage content in the TMX-treated groups as compared to the control group, but these differences were also not statistically significant (Figure 5E–H). The relative level of blood vessel perfusion, assessed via lectin injection, was similar for the three groups (Figure S6F, Supporting Information).

3. Discussion

Fibrotic tumors display a dense stromal matrix, which contributes to poor prognosis and hinders the accumulation of drugs and drug delivery systems.^[41] Recent studies investigated the modulatory effect of TMX on the TME in fibrotic pancreatic tumors (i.e., changes in gene expression and protein content in tumors) and suggest that TMX holds potential for repurposing as TME remodeling agent.^[37] We here set out to study the capability of TMX to modulate the TME and improve tumor-targeted drug delivery. We investigated the ability of TMX, in free and micellar form, to prime the TME in prototypic pancreatic (PANC-1) and triple-negative breast cancer (4T1) models. This was done by extensive microscopy and by visualizing and quantifying the tumor accumulation of clinically relevant fluorophore-labeled nanocarriers (Cy7-CCPM). Our findings show that TMX induces a very modest and statistically non-significant modulation of the TME in PANC-1 and 4T1 tumors, and does not improve the tumor accumulation of Cy7-CCPM in any of the two models.

TMX in free form has a very low aqueous solubility (Log $P = 6.35$). It is orally administered in patients and typically i.p. in-

jected in preclinical studies. After oral application, about 50% of TMX is metabolized in the liver, and its most active derivative (4-hydroxytamoxifen) is subjected to rapid clearance.^[42] To improve the in vivo availability and target site accumulation of TMX, we developed a nanoformulation of TMX. This formulation is based on π electron-stabilized polymeric micelles, which have been previously shown to display high physicochemical stability and excellent loading capacity and retention of aromatic group-containing hydrophobic drugs.^[43–45] Using this platform, we were able to increase TMX concentration in the micelles to values above 10 mg mL⁻¹. This allowed us to administer 50 mg kg⁻¹ of TMX i.v., which is comparable to the doses typically injected i.p. to mice,^[46,47] and far above (5-fold) the i.v.-administered doses previously used preclinically.^[42,48] Thus, through our nanoformulation, we were able to administer TMX i.v. in a colloidal suspension in water-based media at a dose that can otherwise only be applied i.p. in oil-based solvent. Moreover, based on the lack of body weight loss observed upon i.v. administration of up to nine doses of TMX-loaded micelles, it can be concluded that our TMX nanoformulation has a good profile in preclinical mouse models.

Interestingly, in pancreatic and breast cancer mouse models, we observed slightly yet significantly faster tumor growth upon treatment with both free and micelle-loaded TMX as compared to saline controls. This might limit the future application of TMX as a stromal remodeling agent. TMX is clinically used for the treatment of ER-positive breast cancer, where it inhibits tumor growth via modulating ER-dependent proliferation signaling.^[49,50] When administered for the treatment of ER-negative tumors, TMX does

not usually reduce tumor sizes,^[51] and at times even induces cell proliferation.^[52] 4T1 is a TNBC model, where ER is lacking and where TMX-mediated tumor growth inhibition would thus not be expected. As reported elsewhere, ER is also not detected in PANC-1 cells.^[53] Somewhat to our surprise, however, we observed faster tumor growth upon TMX treatment in both tumor models. However, this was not supported by the microscopic analysis of Ki67, which showed similar levels of the proliferation marker between the groups for both tumor models. Previous findings have linked the effect of TMX on tumor growth to signaling by the non-canonical G protein-coupled estrogen receptor (GPER), and reported that TMX-induced TNBC growth can be prevented by the knockdown of GPER.^[52,54] In a pancreatic cancer mouse model, TMX-mediated modulation of the tumor stroma has been attributed to mechanisms involving GPER signaling (and independent of ER α/β).^[36] Although the mechanism behind the observed TMX-induced tumor growth needs further clarification, we hypothesize that GPER-modulating effects may play a role in the observed phenomenon. This is consistent with our preliminary western blot analysis of lysed PANC-1 and 4T1 tumor tissue, which suggests the presence of GPER in both tumor models (Figure S8, Supporting Information). A more detailed analysis of the molecular mechanisms of TMX treatment on tumor cells and tumor stroma in non-ER-expressing cancers is warranted, but goes beyond the scope of the present work.

Multiple previous studies have indicated that TMX can act as a microenvironment-modulating agent. TMX exhibited remodeling activity in the stroma of healthy mammary tissues in female rats,^[55] and most prominently, TMX remodeled the TME in pancreatic tumors in mice.^[35,37] These findings led us to explore TMX-modulation of the stroma in desmoplastic pancreatic and TNBC tumors. Overall, there was no strong effect of TMX priming in any of the two assayed models, with only very minor and statistically non-significant changes in collagen deposition, in the amount of tumor blood vessels, and in the amount of tumor-associated macrophages.

Our results are not in line with the study of Cortes et al., who noted a strong dose-dependent reduction in collagen content upon TMX administration, as well as potent downregulation of the enzyme responsible for collagen crosslinking (i.e., lysyl oxidase; LOX).^[37] However, a different pancreatic tumor model (transgenic KPC mice) was used, and also the TMX doses were different. As a matter of fact, mice were treated daily with fairly high doses of TMX (100–250 mg kg⁻¹), for a total of 8–14 days.^[37] In our study, mice only received 50 mg kg⁻¹ of TMX every other day, which is more in line with what can be realistically achieved in patients in a clinical setting.^[56] While we understand that the lower dose used compromises a fair comparison with the original preclinical reference study, we ensured to systematically compare the activity of our micellar TMX formulation with the one of the free drug. In fact, any attempt to increase the drug concentration in the micelles beyond the selected dose of 50 mg kg⁻¹ resulted in drug precipitation and micelle instability.

At this more reasonable dosing level, the low TMX-mediated TME modulation did not increase the tumor accumulation of Cy7-CCPM. In none of the tested models, and neither in vivo nor ex vivo, there were indications that TMX priming has a beneficial effect on nanomedicine tumor targeting. Overall, we did observe slightly higher CCPM accumulation in PANC-1 tu-

mors as compared to 4T1 tumors as a result of passive targeting, that is, not induced by TME modulation by TMX. Given the comparable levels of blood vessel density and perfusion in both models, it seems plausible that the threefold higher amount of tumor-associated macrophages, which have been recognized as a nanoparticle reservoir in (or hitchhiker to) solid tumors,^[57–59] may explain the higher accumulation of the polymeric drug delivery system in PANC-1 tumors.

Altogether, our results illustrate that TMX is not suitable for pharmacological TME priming in PANC-1 pancreatic and 4T1 triple-negative breast cancer mouse models for enhanced drug delivery. While TMX might show TME-modulating properties in other types of fibrotic cancers, further analyses are needed to identify efficacious anti-fibrotic compounds that can modulate the stroma in PANC-1 pancreatic and 4T1 TNBC desmoplastic tumors to improve drug delivery and drug therapy outcomes.

4. Conclusion

We show that TMX, both in free and micelle-encapsulated form, does not have a strong impact on the composition of the TME in PANC-1 pancreatic and 4T1 triple-negative breast cancer mouse models. This lack of effect on the tumor stroma likely explains the absence of TMX-mediated improvement in the tumor accumulation of core-crosslinked polymeric micelles, which were used as a clinically relevant drug delivery system. Altogether, our findings indicate that TMX priming may not be beneficial for tumor-targeted drug delivery. To which extent it can help to improve the accumulation and performance of standard (chemo)therapeutics needs to be explored in separate studies, to eventually enable a more comprehensive and complete understanding of its repurposed TME priming potential.

5. Experimental Section

Tamoxifen Formulation and Characterization: All experiments were performed by using an active metabolite of TMX ((Z)-4-hydroxytamoxifen, Peprrotech, Germany), which displays a 25–100-fold higher affinity for the ER than the parent drug.^[60,61] TMX-loaded polymeric micelles composed of mPEG-*b*-p(HPMAm-Bz) copolymer were formulated by using the nanoprecipitation method.^[38] To prepare polymeric micelles with 1:10 w/w drug/polymer ratio, 2 mg of TMX and 20 mg of polymer were dissolved in THF. The solution was sonicated in an ultrasonic bath (VWR International, Germany) for 5–10 min and added to 1 mL of Milli-Q water under stirring. The mixture was kept at RT for 48 h to allow the evaporation of THF and the resulting formulation was filtered using hydrophilic nylon membranes (pore size: 0.45 μ m). Micelles were characterized via DLS (Nano-s, Malvern Instruments Ltd., UK) for assessing the size (hydrodynamic diameter) and Pdl. Furthermore, the amount of THF residue in the micelles was analyzed via headspace gas chromatography (HS-GC). TMX concentration was determined by HPLC (Waters, MA, USA) and the EE% was calculated as follows in Equation (1):

$$EE\% = \frac{\text{detected amount of drug}}{\text{feed amount of drug}} \times 100 \quad (1)$$

The stability (size, drug retention) of the micelles was monitored for 7 days at RT or at 4 °C. In addition, in vitro drug release study was performed at 37 °C using a Float-A-Lyzer G2 dialysis membrane (MWCO of 300 KDa, Spectrum Labs) in PBS (Life Technology, Germany) with the addition of

45 mg mL⁻¹ BSA (PAN Biotech, Germany). Samples were collected at 0, 1, 4, 24, 48, 72, and 96 h and the retained drug was quantified via HPLC measurements.

Micelles were concentrated using a centrifugal concentrator (Vivaspin; Sartorius, Germany) for 20 min until reaching a minimum concentration of 10 mg mL⁻¹. The size and drug amount were determined by DLS and HPLC, respectively. Prior to in vivo administration, 0.9% NaCl was added to the concentrated solution to maintain blood osmolarity and the formulation was filtered through a 0.2 μm sterile filter.

Cy7-CCPM were generated as described before.^[40]

Cell Culture: PANC-1 human pancreatic cancer cells (American Type Culture Collection, Manassas, VA, USA) were cultured in DMEM medium (Gibco, Life Technologies GmbH, Germany) containing 10% fetal bovine serum (FBS; Life Technologies GmbH, Germany), 1% penicillin/streptomycin (10 000 U mL⁻¹ penicillin and 10 mg mL⁻¹ streptomycin; Sigma Aldrich, Germany), and 1% L-glutamine (Life Technologies GmbH, Germany). hPSCs (ScienCell, Carlsbad, USA) were cultured in Stelate Cell medium (SteCM; ScienCell, Carlsbad, USA) supplemented with 2% FBS (ScienCell, Carlsbad, USA), 1% penicillin/streptomycin (ScienCell, Carlsbad, USA), 1% L-glutamine (ScienCell, Carlsbad, USA). 4T1 breast cancer cells (American Type Culture Collection, Manassas, VA, USA) were cultured in RPMI medium (RPMI 1640; Gibco, Life Technologies GmbH, Germany), supplemented with 10% FBS (Life Technologies GmbH, Germany), 1% penicillin/streptomycin (Life Technologies GmbH, Germany). Cells were maintained at 37 °C in a humidified incubator with 5% CO₂.

In Vivo Therapy Study: All animal experiments were approved by governmental committee for laboratory animal care and use (LANUV [Recklinghausen, Germany]) and conducted in accordance with the federal German law and European directive 2010/63/EU on the protection of animals used for scientific procedures. The experiments were also in compliance with the ARRIVE guidelines and the Guide for the Care and Use of Laboratory Animals. 8-10-week-old mice were housed under specific pathogen-free conditions, with controlled temperature and 12 h light/dark cycles, and food and water were given ad-libitum.

PANC-1 pancreatic cancer cells (2 × 10⁶) and hPSC (2 × 10⁶) were subcutaneously co-injected into the left flank of male BALB/c SCID mice (n = 15), as described elsewhere.^[62] 4T1 breast cancer cells (2.5 × 10⁴) were orthotopically inoculated into the right abdominal mammary gland fat pad of female BALB/cAnNRj mice (n = 15). The start (day 5 and day 3 post-cell injection for the pancreatic and the breast cancer model, respectively) and the duration of the treatment regimen were set according to the characteristics of the model, tumor growth rate, and health conditions of the mice. Mice were randomly divided in three groups (n = 5 mice per group) and administered every 48 h with either i) 50 mg kg⁻¹ of free TMX dissolved in corn oil (i.p., TMX free group), ii) 50 mg kg⁻¹ of TMX loaded in polymeric micelles (i.v., TMX micelle group), or iii) 0.9% NaCl sterile solution (i.v., control group), continuing until mice reached humane endpoints. All i.v. injections were performed on anesthetized mice using a catheter consisting of a 30 G cannula (B. Braun, Melsungen, Germany) and a polyethylene tube (Hartenstein, Würzburg, Germany). Inhalation anesthesia was induced in an anesthetic chamber (Drägerwerk AG, Lübeck, Germany) using 5 Vol% isoflurane (Forene, Abbott, Wiesbaden, Germany) in oxygen-enriched air using a dedicated vaporizer, and maintained at 2–2.5 Vol% during the injections. i.p. injections were performed using a sterile syringe with a 27 G cannula (B. Braun, Melsungen, Germany). Mice weight and behavior were monitored daily throughout the whole study. The variation of mice weight was calculated as percentage of the body mass of each mouse on day 0. The tumor size was evaluated daily via caliper measurements (width, w and length, l), and weekly via in vivo CT assessments. According to the xenograft tumor model protocol,^[63] the tumor volume was calculated as follows (Equation (2)):

$$V = w^2 \times \frac{l}{2} \quad (2)$$

Biodistribution Study: After five and nine doses of therapy for PANC-1 and 4T1 models, respectively, mice were administered with Cy7-labeled CCPM (2 nmol; in 50 μL 0.9% NaCl sterile solution). All imaging proce-

dures were performed on anesthetized mice and Bepanthen eye ointment (Bayer Vital GmbH, Germany) was applied to prevent eye dehydration. The biodistribution of fluorescent CCPM was longitudinally imaged in vivo using a hybrid μCT-FLT device (U-CT OI, MLLabs B.V., Utrecht, the Netherlands). ≈130 scan points were acquired using an FLT laser and filter with excitation and emission wavelengths at 730 and 775 nm, respectively. Afterward, 480 projections were acquired with an x-ray tube voltage of 55 kV, power 0.17 mA, and exposure time of 75 ms. Scans were acquired before injecting Cy7-CCPM and at 0.25, 4, 24, and 48 h post-injection. On the last day of the experiment, FITC lectin was injected i.v. to the mice prior to sacrifice, to identify functional and perfused vessels. Organs were resected for further ex vivo analyses and 2D FRI of the resected organs (brain, lungs, kidneys, liver, spleen, tumors) were acquired using a 750 nm excitation wavelength in the fluorescence molecular tomography (FMT) device (FMT 400, PerkinElmer, Waltham, MA, USA).

CT-FLT and FRI Image Analysis: All 3D CT images were reconstructed with a Feldkamp type algorithm (filtered back-projection). 3D fluorescence reconstructions were produced from the automatic generation of shape, scattering maps and absorption maps.^[64] Heart, lungs, liver, spleen, kidneys, and tumors were segmented for all mice at all time-points post-injection from the CT data using Imaalytics Preclinical 3.0 (Gremse-IT GmbH, Germany). The concentration (%ID g⁻¹) of Cy7-CCPM in the organs was calculated as a fraction of the total fluorescence signal measured in the FLT scans at 0.25 h post-injection, and considering a density of 1 g cm⁻³. 2D FRI images were segmented using Imaalytics Preclinical 3.0 and the mean fluorescence values in each organ were plotted for all mice. To visually compare the fluorescent signal between all tumors and organs the fluorescent scale was adjusted in a range of 0–0.5 for the 3D CT-FLT images, and 0–0.3 for 2D FRI.

Histological Characterization of the Tumor Microenvironment: After ex vivo imaging, tumors were embedded in optimal cutting temperature matrix compound (Tissue-Tek OCT) for cryosection staining, and preserved at –80 °C. Eight μm-thick cryosections were fluorescently stained following a standard experimental procedure. The slices were washed with PBS, fixed with 80% methanol at RT and with –20 °C acetone, and additionally washed with PBS. Rat anti-CD31 (1:100; BD-Biosciences, USA), rat anti-F4/80 (1:50; Bio-Rad, Germany), rabbit anti-collagen I (1:100; Novus Biologicals, USA), rabbit anti-collagen (1:100; Origene, USA), rabbit anti-Ki67 (1:500; Abcam, UK), mouse anti-αSMA biotinylated (1:100; Progen) primary antibodies diluted in 12% BSA were applied to the slices for 1 h at RT. The excess amount of primary antibody was removed via PBS washing and the slides were incubated with the respective secondary antibodies (Cy3 anti-rat; 1:500, Cy3 anti-rabbit; 1:500; Dianova, Germany, Cy3 streptavidin anti-biotin; 1:500; Abcam, UK) together with DAPI (nuclei staining; 1:500; Merck, Germany) diluted in 12% BSA for 45 min at RT. Tumor sections were washed with PBS, mounted with Mowiol 4–88 (anti-fade agent; Carl-Roth, Germany) and glass-covered. A slightly different protocol was used for F4/80 staining on pancreatic tumors: after slices fixation, blocking step was performed with 10% rabbit serum containing 0.1% Triton X-100 (Sigma-Aldrich, Germany) for 1 h. Slides were subsequently washed with PBS and incubated with the rat anti-F4/80 (1:50; Bio-Rad, Germany) primary antibody diluted in PBS overnight at 4 °C. The excess amount of antibody was washed out with PBS, and horseradish peroxidase (HRP) anti-rat secondary antibody (1:500; Abcam, UK) diluted in PBS was applied for 1 h at RT. A Cy7 tyramide signal amplification (TSA)-conjugated dye (1:50; PerkinElmer, USA) diluted in the appropriate amplification diluent buffer (PerkinElmer, USA) was applied for 10 min, and slides were incubated with PBS diluted DAPI (1:500; Merck, Germany) for 10 min. Another protocol was used for LOX staining: after fixation, a blocking step was performed by adding a ready-to-use antibody diluent and blocking buffer formulation optimized specifically for TSA immunohistochemistry protocols (PerkinElmer, USA) at RT for 1 h. Slides were subsequently incubated with the rabbit anti-LOX (1:500; Novus Biologicals, Germany) primary antibody diluted in PBS at RT for 2 h. The slides were washed with PBS, and HRP anti-rabbit secondary antibody (1:200; Abcam, UK) diluted in PBS was applied for 45 min at RT. A Cy5 TSA-conjugated dye (1:100; PerkinElmer, USA) diluted in the appropriate amplification diluent buffer (PerkinElmer, USA) was applied for 10 min. Slides were washed with PBS

and finally mounted with mowiol mixed with DAPI (1:500; Merck, Germany). Hematoxylin and eosin (H&E) were consecutively applied on tumor sections previously fixed in 4% paraformaldehyde (PFA) according to standard procedures. The excess of hematoxylin dye was removed using 0.1% HCl and tap water. The sections were dehydrated with different gradients of ethanol (from 70% to 96% and 100%) and xylene, mounted with Vitro-clud (R. Langenbrinck GmbH, Germany) and covered with cover slips.

Microscopy and Image Analysis: Images of the fluorescently stained slides were acquired using an AxioImager M2 microscopy system with an AxioCamMRm Rev.3 camera (Carl Zeiss AG, Jena, Germany). Eight representative images per tumor were taken using similar exposure time settings for each channel in different stainings. Images with a magnification of 200 \times were acquired in the “periphery” and “core” areas of the tumors, and the necrotic part was neglected. The area fraction (%) of the respective signal was quantified with the AxioVision SE64 Rel. 4.8 software. Overviews in 40 \times of whole sections were acquired in the bright-field channel for the H&E stained tumors using the Vectra 3.0.5 microscope (PerkinElmer, USA). The necrotic part was identified and segmented with Imalytics Preclinical 3.0 based on different voxel intensity of the intact part versus the disintegrated cytoplasmic components. One hundred μ m-thick, unstained and water-immersed sections were scanned via TPLSM using the FV1000MPE multiphoton microscope (Olympus, Germany). Four image stacks of 50 images with a step size of 1 μ m were acquired per each tumor and processed using the Imaris software (Bitplane AG, Switzerland) for the quantification of collagen content (generated via SHG imaging) and lectin volume (fluorescence signal was obtained through the photomultiplier filters adjusted to 490–540 nm spectra). Same threshold and exposure time settings for collagen and lectin were selected for all samples. The thickness of the collagen fibers was quantified using the BoneJ plugin in the image processing package Fiji.

Statistical Analysis: All polymeric micelles characterization experiments were performed in triplicate. 3D CT-FLT and 2D FRI images were obtained from all mice/tumors/organs of each study group ($n = 5$ mice per group). All immunofluorescence histological analyses were performed on two sections per tumor sample and 4 representative images were acquired per each fluorescently stained section. Four images per tumor were obtained via TPLSM imaging. All bars in the graphs represent averages per group (data points represent individual mouse values) and are plotted with their respective standard deviation using GraphPadPrism 9 (Graph-Pad Software, USA). 0.05 was used as alpha threshold for determining statistical significances which were considered for p values < 0.05 (*), $p < 0.01$ (**), and $p < 0.001$ (***) .

Unpaired nonparametric one-way ANOVA analysis with Dunn’s multiple comparison test was performed for comparing the size, Pdl and EE of TMX micelles, as well as for comparing the tumor volumes. The same statistical analysis was performed for in vivo and ex vivo fluorescence signal analysis, and for the area fractions of CD31, F4/80, and collagen in the fluorescence stainings, as well as in the fiber thickness, collagen, and perfusion volume analyses.

Supporting Information

Supporting Information is available from the Wiley Online Library or from the author.

Acknowledgements

The authors gratefully acknowledge financial support by the European Research Council (ERC-CoG: Meta-Targeting 864121), by the German Research Foundation (DFG: GRK2375 (grant number 331065168), LA-2937/4-1 and SFB1066), and by the German Federal Ministry of Research and Education (BMBF: Gezielter Wirkstofftransport; PP-TNBC, Project No. 16GW0319K). Support by the Two-Photon Imaging Core Facility at the Interdisciplinary Center for Clinical Research (IZKF) at the Faculty of Medicine at RWTH Aachen University is also acknowledged. The table of contents image was created by using BioRender.com.

Open access funding enabled and organized by Projekt DEAL.

Conflict of Interest

The authors declare no conflict of interest.

Data Availability Statement

The data that support the findings of this study are available from the corresponding author upon reasonable request.

Keywords

drug delivery, nanomedicine, polymeric micelles, tamoxifen, tumor microenvironment

Received: March 16, 2023

Revised: June 27, 2023

Published online:

- [1] R. Baghban, L. Roshangar, R. Jahanban-Esfahlan, K. Seidi, A. Ebrahimi-Kalan, M. Jaymand, S. Kolahian, T. Javaheri, P. Zare, *Cell Commun. Signaling* **2020**, *18*, 59.
- [2] I. F. Tannock, C. M. Lee, J. K. Tunggal, D. S. M. Cowan, M. J. Egorin, *Clin. Cancer Res.* **2022**, *8*, 878.
- [3] E. Henke, R. Nandigama, S. Ergün, *Front. Mol. Biosci.* **2020**, *6*, 160.
- [4] R. Rimal, P. Desai, R. Daware, A. Hosseinnejad, J. Prakash, T. Lammers, S. Singh, *Adv. Drug Delivery Rev.* **2022**, *189*, 114504.
- [5] M. Yamauchi, D. L. Gibbons, J. M. Kurie, M. Yamauchi, T. H. Barker, D. L. Gibbons, J. M. Kurie, *J. Clin. Invest.* **2018**, *128*, 16.
- [6] M. U. Munir, *Cancers (Basel)* **2022**, *14*, 2904.
- [7] I. A. Khawar, J. H. Kim, H. J. Kuh, J. *Controlled Release* **2015**, *201*, 78.
- [8] S. Azzi, J. K. Hebda, J. Gavard, *Front. Oncol.* **2013**, *3*, 211.
- [9] T. P. Padera, B. R. Stoll, J. B. Tooredman, D. Capen, E. Di Tomaso, R. K. Jain, *Nature* **2004**, *427*, 695.
- [10] C. H. Heldin, K. Rubin, K. Pietras, A. Östman, *Nat. Rev. Cancer* **2004**, *4*, 806.
- [11] M. Erkan, S. Hausmann, C. W. Michalski, A. A. Fingerle, M. Dobritz, J. Kleeff, H. Friess, *Nat. Rev. Gastroenterol. Hepatol.* **2012**, *9*, 454.
- [12] A. S. Cazet, M. N. Hui, B. L. Elsworth, S. Z. Wu, D. Roden, C. Chan, J. N. Skhinas, R. Collot, J. Yang, K. Harvey, M. Z. Johan, C. Cooper, R. Nair, D. Herrmann, A. Mcfarland, N. Deng, M. Ruiz-borrego, F. Rojo, J. M. Trigo, S. Bezares, R. Caballero, E. Lim, P. Timpson, S. O. Toole, D. N. Watkins, T. R. Cox, M. S. Samuel, M. Martin, A. Swarbrick, *Nat. Commun.* **2018**, *9*, 2897.
- [13] B. W. Miller, J. P. Morton, M. Pinese, G. Saturno, N. B. Jamieson, E. McGhee, P. Timpson, J. Leach, L. McGarry, E. Shanks, P. Bailey, D. Chang, K. Oien, S. Karim, A. Au, C. Steele, C. R. Carter, C. McKay, K. Anderson, T. R. J. Evans, R. Marais, C. Springer, A. Biankin, J. T. Erler, O. J. Sansom, *EMBO Mol. Med.* **2015**, *7*, 1063.
- [14] T. Ojha, V. Pathak, Y. Shi, W. E. Hennink, C. T. W. Moonen, G. Storm, F. Kiessling, T. Lammers, *Adv. Drug Delivery Rev.* **2017**, *119*, 44.
- [15] F. Bochner, V. Mohan, A. Zinger, O. Golani, A. Schroeder, I. Sagi, M. Neeman, *Int. J. Cancer* **2020**, *146*, 2209.
- [16] Y. Zhou, X. Chen, J. Cao, H. Gao, *J. Mater. Chem. B* **2020**, *8*, 6765.
- [17] A. M. Sofias, F. De Lorenzi, Q. Peña, A. A. Shalmani, M. Vucur, J.-W. Wang, F. Kiessling, Y. Shi, L. Consolino, G. Storm, T. Lammers, *Adv. Drug Delivery Rev.* **2021**, *175*, 113831.
- [18] W. Zhen, R. R. Weichselbaum, W. Lin, *Adv. Mater.* **2022**, *35*, 2206370.

- [19] C. J. F. Rijcken, F. De Lorenzi, I. Biancacci, R. G. J. M. Hanssen, M. Thewissen, Q. Hu, F. Atrafi, R. M. J. Liskamp, R. H. J. Mathijssen, I. H. C. Miedema, C. W. Menke – van der Houven van Oordt, G. A. M. S. van Dongen, D. J. Vugts, M. Timmers, W. E. Hennink, T. Lammers, *Adv. Drug Delivery Rev.* **2022**, *191*, 114613.
- [20] V. Torchilin, *Adv. Drug Delivery Rev.* **2011**, *63*, 131.
- [21] D. Peer, J. M. Karp, S. Hong, O. C. Farokhzad, R. Margalit, R. Langer, *Nat. Nanotechnol.* **2007**, *2*, 751.
- [22] X. Wang, J. Luo, L. He, X. Cheng, G. Yan, J. Wang, R. Tang, *J. Colloid Interface Sci.* **2018**, *525*, 269.
- [23] H. Zhou, Z. Fan, J. Deng, P. K. Lemons, D. C. Arhontoulis, W. B. Bowne, H. Cheng, *Nano Lett.* **2016**, *16*, 3268.
- [24] A. Zinger, L. Koren, O. Adir, M. Poley, M. Alyan, Z. Yaari, N. Noor, N. Krinsky, A. Simon, H. Gibori, M. Krayem, Y. Mumblat, S. Kasten, S. Ofir, E. Fridman, N. Milman, M. M. Lübtow, L. Liba, J. Shklover, J. Shainsky-Roitman, Y. Binenbaum, D. Hershkovitz, Z. Gil, T. Dvir, R. Luxenhofer, R. Satchi-Fainaro, A. Schroeder, *ACS Nano* **2019**, *13*, 11008.
- [25] X. Han, Y. Li, Y. Xu, X. Zhao, Y. Zhang, X. Yang, Y. Wang, R. Zhao, G. J. Anderson, Y. Zhao, G. Nie, *Nat. Commun.* **2018**, *9*, 3390.
- [26] M. Panagi, F. Mpekris, P. Chen, C. Voutouri, Y. Nakagawa, J. D. Martin, T. Hiroi, H. Hashimoto, P. Demetriou, C. Pierides, R. Samuel, A. Stylianou, C. Michael, S. Fukushima, P. Georgiou, P. Papageorgis, P. C. Papaphilippou, L. Koumas, P. Costeas, G. Ishii, M. Kojima, K. Kataoka, H. Cabral, T. Stylianopoulos, *Nat. Commun.* **2022**, *13*, 7165.
- [27] Y. Zhang, X. Han, G. Nie, *Nat. Protoc.* **2021**, *16*, 405.
- [28] S. Li, Y. Zhang, J. Wang, Y. Zhao, T. Ji, X. Zhao, Y. Ding, X. Zhao, R. Zhao, F. Li, X. Yang, S. Liu, Z. Liu, J. Lai, A. K. Whittaker, G. J. Anderson, J. Wei, G. Nie, *Nat. Biomed. Eng.* **2017**, *1*, 667.
- [29] V. P. Chauhan, J. D. Martin, H. Liu, D. A. Lacorre, S. R. Jain, S. V. Kozin, T. Stylianopoulos, A. S. Mousa, X. Han, P. Adstamongkonkul, Z. Popović, P. Huang, M. G. Bawendi, Y. Boucher, R. K. Jain, *Nat. Commun.* **2013**, *4*, 2516.
- [30] B. Diop-Frimpong, V. P. Chauhan, S. Krane, Y. Boucher, R. K. Jain, *Proc. Natl. Acad. Sci. U. S. A.* **2011**, *108*, 2909.
- [31] L. Zhang, Y. Wang, Y. Yang, Y. Liu, S. Ruan, Q. Zhang, X. Tai, J. Chen, T. Xia, Y. Qiu, H. Gao, Q. He, *ACS Appl. Mater. Interfaces* **2015**, *7*, 9691.
- [32] T. Cai, J. Jiang, W. Yao, Y. Hu, S. Kong, Q. Fan, X. Yan, F. Li, Z. Shi, *Biomed. Pharmacother.* **2023**, *157*, 114015.
- [33] R. Kato, K. Haratani, H. Hayashi, K. Sakai, H. Sakai, H. Kawakami, K. Tanaka, M. Takeda, K. Yonesaka, K. Nishio, K. Nakagawa, *Br. J. Cancer* **2021**, *124*, 914.
- [34] S. T. Pearce, H. Liu, V. C. Jordan, *J. Biol. Chem.* **2003**, *278*, 7630.
- [35] E. Cortes, D. Lachowski, A. Rice, S. D. Thorpe, B. Robinson, G. Yeldag, D. A. Lee, L. Ghemtio, K. Rombouts, A. E. del Río Hernández, *Oncogene* **2019**, *38*, 2910.
- [36] E. Cortes, M. Sarper, B. Robinson, D. Lachowski, A. Chronopoulos, S. D. Thorpe, D. A. Lee, A. E. Río Hernández, *EMBO Rep.* **2019**, *20*, e46556.
- [37] E. Cortes, D. Lachowski, B. Robinson, M. Sarper, J. S. Teppo, S. D. Thorpe, T. J. Lieberthal, K. Iwamoto, D. A. Lee, M. Okada-Hatakeyama, M. T. Varjosalo, A. E. Río Hernández, *EMBO Rep.* **2019**, *20*, e46557.
- [38] Y. Shi, R. Van Der Meel, B. Theek, E. Oude Blenke, E. H. E. Pieters, M. H. A. M. Fens, J. Ehling, R. M. Schifflers, G. Storm, C. F. Van Nostrum, T. Lammers, W. E. Hennink, *ACS Nano* **2015**, *9*, 3740.
- [39] I. Biancacci, F. De Lorenzi, B. Theek, X. Bai, J. May, L. Consolino, M. Baues, D. Moeckel, F. Gremse, S. Von Stillfried, A. El Shafei, K. Benderski, A. A. Shalmani, A. Wang, J. Momoh, Q. Peña, E. M. Buhl, J. Buyel, W. Hennink, *Adv. Sci.* **2022**, *9*, 2103745.
- [40] I. Biancacci, Q. Sun, D. Möckel, F. Gremse, S. Rosenhain, F. Kiessling, M. Bartneck, Q. Hu, M. Thewissen, G. Storm, W. E. Hennink, Y. Shi, C. J. F. Rijcken, T. Lammers, A. Marios, *J. Controlled Release* **2020**, *328*, 805.
- [41] H. Laklai, Y. A. Miroshnikova, M. W. Pickup, E. A. Collisson, G. E. Kim, A. S. Barrett, R. C. Hill, J. N. Lakins, D. D. Schlaepfer, J. K. Mouw, V. S. LeBleu, N. Roy, S. V. Novitskiy, J. S. Johansen, V. Poli, R. Kalluri, C. A. Iacobuzio-Donahue, L. D. Wood, M. Hebrok, K. Hansen, H. L. Moses, V. M. Weaver, *Nat. Med.* **2016**, *22*, 497.
- [42] C. M. Buchanan, N. L. Buchanan, K. J. Edgar, J. L. Little, M. O. Malcom, K. M. Ruble, V. J. Wachter, M. F. Wempe, *J. Pharm. Sci.* **2007**, *96*, 644.
- [43] H. Cabral, K. Kataoka, *J. Controlled Release* **2014**, *190*, 465.
- [44] Y. Shi, M. J. van Steenberg, E. A. Teunissen, L. Novo, S. Gradmann, M. Baldus, C. F. van Nostrum, W. E. Hennink, *Biomacromolecules* **2013**, *14*, 1826.
- [45] W.-R. Zhuang, Y. Wang, P.-F. Cui, L. Xing, J. Lee, D. Kim, H.-L. Jiang, Y.-K. Oh, *J. Controlled Release* **2019**, *294*, 311.
- [46] K. B. Andersson, L. H. Winer, H. K. Mørk, J. D. Molkenin, F. Jaisser, *Transgenic Res.* **2010**, *19*, 715.
- [47] F. Denk, L. M. Ramer, E. L. K. S. Erskine, M. A. Nassar, Y. Bogdanov, M. Signore, J. N. Wood, S. B. McMahon, M. S. Ramer, *Acta Neuropathol. Commun.* **2015**, *3*, 74.
- [48] Z. Yang, Q. Chen, J. Chen, Z. Dong, R. Zhang, J. Liu, Z. Liu, *Small* **2018**, *14*, 1803262.
- [49] C. K. Osborne, K. Hobbs, G. M. Clark, *Cancer Res.* **1985**, *45*, 584.
- [50] G. Yang, S. Nowsheen, K. Aziz, A. G. Georgakilas, *Pharmacol. Ther.* **2013**, *139*, 392.
- [51] G. Ma, G. Ma, J. He, Y. Yu, Y. Xu, X. Xu, Y. J. Martinez, D. M. Lonard, J. Xu, J. Xu, *Int. J. Biol. Sci.* **2015**, *11*, 618.
- [52] S. Manna, M. K. Holz, *Signal Transduction Insights* **2016**, *5*, ST1.S2901.
- [53] X. Xie, M. Y. Wu, L. M. Shou, L. P. Chen, F. R. Gong, K. Chen, D. M. Li, W. M. Duan, Y. F. Xie, Y. X. Mao, W. Li, M. Tao, *Oncol. Lett.* **2015**, *9*, 837.
- [54] O. Treeck, S. Schüler-Toprak, O. Ortmann, *Cells* **2020**, *9*, 2358.
- [55] R. Hattar, O. Maller, S. McDaniel, K. C. Hansen, K. J. Hedman, T. R. Lyons, S. Lucia, R. S. Wilson, P. Schedin, *Breast Cancer Res.* **2009**, *11*, R5.
- [56] M. Pein, T. Oskarsson, *EMBO Rep.* **2019**, *20*, e47334.
- [57] M. A. Miller, Y. Zheng, S. Gadde, C. Pfirschke, H. Zope, C. Engblom, R. H. Kohler, Y. Iwamoto, K. S. Yang, B. Askevold, N. Kolishetti, M. Pittet, S. J. Lippard, O. C. Farokhzad, R. Weissleder, *Nat. Commun.* **2015**, *6*, 8692.
- [58] A. M. Sofias, Y. C. Toner, A. E. Meerwaldt, M. M. T. Van Leent, G. Soultanidis, M. Elschot, H. Gonai, K. Grendstad, Å. Flobak, U. Neckmann, C. Wolowczyk, E. L. Fisher, T. Reiner, C. D. L. Davies, G. Bjørkøy, A. J. P. Teunissen, J. Ochando, C. Pérez-Medina, W. J. M. Mulder, S. Hak, *ACS Nano* **2020**, *14*, 7832.
- [59] J. Momoh, D. Kapsokalyvas, M. Vogt, S. Hak, F. Kiessling, M. van Zandvoort, T. Lammers, A. M. Sofias, *Adv. Drug Delivery Rev.* **2022**, *189*, 114528.
- [60] C. Fabian, L. Tilzer, L. Sternson, *Biopharm. Drug Dispos.* **1981**, *2*, 381.
- [61] M. L. Asp, J. J. Martindale, J. M. Metzger, *PLoS One* **2013**, *8*, e78768.
- [62] P. R. Kuinty, R. Bansal, S. W. L. De Geus, D. F. Mardhian, J. Schnittert, J. van Baarlen, G. Storm, M. F. Bijlsma, H. W. van Laarhoven, J. M. Metselaar, P. J. K. Kuppen, A. L. Vahrmeijer, A. Östman, C. F. M. Sier, J. Prakash, *Sci. Adv.* **2019**, *5*, eaax2770.
- [63] Protocol Online, <http://www.protocol-online.org/prot/Protocols/Xenograft-Tumor-Model-Protocol-3810.html> (accessed: Feb 2023).
- [64] F. Gremse, B. Theek, S. Kunjachan, W. Lederle, A. Pardo, S. Barth, T. Lammers, U. Naumann, F. Kiessling, *Theranostics* **2014**, *4*, 960.